Dielectric and Molecular Dynamics Study of the Secondary Relaxations of Poly(styrene-*co*-methylmethacrylate) Copolymers: Influence of the Molecular Architecture

M. Encinar,[1] M.G. Prolongo,[2] R.G. Rubio,[1]* F. Ortega,[1] A. Ahmadi,[3] J.J. Freire.[3]

[1] Departamento de Química Física I, Facultad de Química, Universidad Complutense, 28040-Madrid, Spain. [2] Departamento de Materiales e Ingeniería Aeroespacial, ETSI Aeronáuticos, Univ. Politécnica, 28040-Madrid, Spain. [3] Departamento de Ciencias y Técnicas Fisicoquímicas, Facultad de Ciencias, Universidad Nacional de Educación a Distancia, 28040-Madrid. Spain.

Published in The European Physical Journal E, vol. 34, pp. 134-1/14 (2011)

* Corresponding author: rgrubio@quim.ucm.es

Abstract

The effect of the structure of copolymers (random, alternate or diblock) on their dynamics has been studied by dielectric spectroscopy. Six copolymers of styrene and methyl methacrylate (three diblocks, one alternate and two random) have been studied. The results show that the sub-T_g transitions of the diblock samples can be described by one asymmetric Havriliak-Negami (HN) function, while two are necessary for the rest of the copolymers (β and γ relaxations). The characteristic times of the sub-T_g relaxations show an Arrhenius temperature dependence and there is a strong coupling of the α and β relaxations at high temperatures. The deconvolution of the merging relaxations has been made in the framework of the *Williams Ansatz* set out in terms of Havriliak-Negami distributions. The γ relaxation may be assigned to the rotation of the methyl methacrylate group in a styrene-rich environment. The Molecular Dynamics simulations of a poly(methyl methacrylate) homopolymer and of the alternate copolymer are in qualitative agreement with the experimental results, although they predict smaller values for the activation energy of the sub-T_g relaxations.

I. Introduction

Copolymers have attracted much attention because they can be frequently used to tune the properties of a material between those of the corresponding homopolymers, they may be used as compatibilizers, and, in the case of block copolymers, they form ordered structures at the nanometer scale below the so-called order-disorder transition temperature [1,2]. In the case of copolymers, the final value of a given property, e.g. the melting, T_m, or the glass transition temperature, T_g, do not only depend on the monomer composition, but also on the architecture of the copolymer: random, alternate or block [2,3].

In the case of block copolymers in which the two blocks have well separated T_g's, the dynamics of the low-T_g blocks can be affected by the presence of a rigid phase, thus being rather different than the

dynamics of the corresponding homopolymer [4-9]. In a recent work, using dielectric relaxation and dynamic mechanical spectroscopy techniques, Encinar *et al*. [10] have studied the dynamics of the polystyrene-*b*-poly(*t*-butyl acrylate) (PS-*b*-PtBa) copolymers. They found that the relaxation times of the α relaxation of the PtBa blocks are very close to that of the PtBa homopolymer for temperatures that are below the T_g of PS but still well above that of PtBa. In the case of PS-*co*-PtBa random and alternate copolymers, which were found to be one phase disordered materials, concentration fluctuations of relatively short range played an important role in the dynamic properties leading to a broadening of the dynamic relaxations, an effect which is similar to the one described years ago for polymer blends [11]. Moreover, they found that the existence of a glassy PS phase modified the relaxation times of the β relaxation of the PtBa groups with respect to that of the PtBa homopolymer, a result that was somewhat surprising due to the relatively local character of the sub-glass transition. These conclusions were qualitatively confirmed by Molecular Dynamics simulations that also showed an unusual behavior in the short time range and yielded a semi-quantitative agreement with the experimental data. In recent years the equilibrium properties and phase diagram of diblock copolymers formed by styrene and an *n*-alkyl methacrylate (*n* being the number of carbon atoms of the lateral chain) have been studied in detail because of their departure from the classical behaviour [12-14]. While the copolymers with methyl methacrylate and with $n > 5$ present an order-disorder transition when the temperature is increased, those with $2 \leq n \leq 4$ are unusual because the transition takes place when the temperature is decreased. More recently, Ahn *et al*. [15] have studied the phase behaviour of polystyrene-*b*-poly(methyl methacrylate) (PS-*b*-PMMA). In the case of poly(styrene-*co*-alkyl acrylate) copolymers, the acrylate monomers have a dielectric strength one hundred times higher that of the styrene monomers[16]). Bergman *et al*. [17], and Arbe *et al*. [18] have studied the dynamic behaviour of poly(*n*-alkyl methacrylates) using several experimental techniques. Previous studies by Schmidt-Rohr *et al* [19], and by de Dens *et al*. [20] have pointed out that the origin of the β transition in PMMA is a 180º flip of the OCO plane of the methacrylate group. Moreover, this motion seems to be associated to a distribution of

correlation times that appears to be bimodal with both mobile and immobile side groups. The side-group flip is accompanied by a main-chain rearrangement which corresponds to a random rotation around the local chain axis. More recently, Morais *et al*. have carried out a detailed study of the dynamics of random, alternate and block copolymers made of styrene and methyl methacrylate using dynamical mechanical spectroscopy (DMTA) [21]. In contrast to dielectric experiments, polystyrene and poly(methacrylate) chains show similar responses to mechanical stimuli. Two well differentiated glass transition temperatures were found for two of the three block copolymers studied, while only one was reported for the random, alternate, and one of the block copolymers, and all the samples studied were found to be thermorheologically complex. In order to describe the behaviour of the relaxation functions calculated from the complex Young modulus it was necessary to use two Kohlrausch-Williams-Watts functions for each of the temperatures studied. The bimodal character of the transitions is in agreement with the NMR study of Ref. [19]. Similar conclusions were reached by Ruzette *et al*. for diblock copolymers of styrene and n-alkyl methacrylates in the disordered state and for temperatures well separated from the order-disorder one [12]. They also found thermorheological complexity when the copolymers approached the order-disorder transition from the disordered phase. Pakula and Floudas [22] have shown that, for block copolymers in the ordered state, it is not possible to build master curves for the shear modulus at low frequencies.

The goal of the present work is to study the dynamics of copolymers made of styrene and methyl methacrylate using dielectric spectroscopy, where only the methyl methacrylate monomer is significantly active. The results for diblock, random and alternate copolymers will be compared; both single phase and microphase separated samples have been studied. It will be shown that for the random and alternate copolymers present two sub-T_g dynamic processes, while the block copolymers show only one sub-glass transition in the temperature-frequency range studied. Also, in the case of the block copolymers, the temperature dependence of the relaxation times of the α and β relaxations is different

for the one phase and for the microsegregated samples. Moreover, Dynamic Molecular simulations will be performed to qualitatively compare the trends obtained experimentally for the local transitions.

Due to the proximity of the calorimetric T_g's of PS and PMMA, the analysis of the data in the frequency domain (loss modulus vs. frequency curves) has not allowed to resolve the contributions of the two different dynamic modes found near the glass transition [23-26]. This is a problem frequently found in this type of systems. However, we will point out that the analysis of the data in the time domain makes such a task possible, showing that at low temperatures it is necessary to use two empirical functions to describe the sub T_g behaviour. Above the glass transition, the merging of the segmental and secondary relaxations will be analysed in terms of a *Williams Ansatz* approximation and using Havriliak Negami distributions to describe the time domain relaxation functions.

II. Experimental and Molecular Dynamics Methods

The copolymers were purchased from Polymer Source (Canada). Gel permeation chromatography using tetrahydrofuran as solvent was used to determine the overall molecular weight, and the polydispersity index M_w/M_n. The relative content of the co-monomers was obtained by NMR. The characteristics of the different samples are given in Table 1.

The dielectric spectrometer used was the same of a previous work [28], although in the present work case an Alpha-N Novocontrol analyzer was used in the frequency range from 10^{-2} Hz to 10^6 Hz. A liquid nitrogen cryostat mantained the temperature within ±0.1K. The samples were introduced in a parallel-plate capacitor (0.1 mm thickness and 30 mm in diameter) and kept under vacuum above the T_g of PMMA in order to erase the previous thermal history. All the measurements were carried out in the isothermal mode.

The Molecular Dynamics simulation of atactic PMMA chains and of alternate copolymers chains (with regular stereochemistry so that phenyl and ester groups are placed at the same side along the polymer backbone) was carried out using the second-generation PCFF forcefield [29] without crossed terms. PCFF improves the previous CFF91 forcefield for application to polymers and organic materials in calculations of cohesive energies, mechanical properties, compressibilities, heat capacities and elastic constants. It handles electron delocalization in aromatic rings by means of a charge library rather than bond increments. Simulations were performed for temperatures 500, 600, 700, 800 and 1100 K using a step time of 1 fs, the Berendsen thermostat, periodic boundary conditions and the NVT ensemble. High enough temperatures were chosen to allow for an accurate characterization of the relaxation of local motions within the time range covered by the simulation trajectories. The systems were formed by ten chains each containing ten repeating units (or monomers), and were equilibrated with an initial 5 ns simulation with density of 0.7 g/cm^3 at the highest temperature. Several similar runs were performed to reach the desired temperatures, and then NPT simulations were performed at each temperature so that

the systems acquired a density close to real. The system properties were analysed from the trajectories corresponding to final 5ns NVT production runs, with a step time of 1 fs. These trajectories were saved using recording times in the 5-25 ps range. The analysis focused in the ester groups, in particular the rotational angle, Φ, defined by the –(C-C-C-O)- bonds partially included in the ester moieties and the orientation of the C=O bond. For our atactic PMMA chains we only analysed five ester groups stereochemically placed at a given side (which we define as the dextro, or *d*, stereochemical disposition) along an atactic chain backbone. For the alternate chain we analysed the four groups for which the ester group is between phenyls. The distribution of rotational angles is very similar for both types of chains, showing two minima, separated by a relatively high rotational angle. Considering the *d* stereochemical disposition of the groups, the minima are located at the approximate values Φ= -60º, +120º, separated by a relatively high rotational barrier. This is consistent with the common description of the β relaxation of PMMA chains as a rotation of about 180º around the C-COO bond, i.e. a two-site jump (or flip) [19]. Therefore, we have tried to explain the different experimental behaviors of homopolymer and alternate copolymers by studying the time evolution of the C=O orientation along our dynamic trajectories, since it has been demonstrated time ago that the dipole moment of the ester group is nearly antiparallel to this bond vector [30].

III. Results and Discussion

The set of samples studied in this work have been previously characterized by means of differential scanning calorimetry and dynamic mechanical analysis [21]. In that work (see Table 2 and Fig. 1 of Reference [21]), it was observed that two of the diblock copolymers (D2 and D3) showed two separate glass transitions as a consequence of their microphase segregated nature. On the other hand, the D1 sample (with the smallest PMMA block) shows only one T_g and it was found to be homogeneous at the level of a 10 nm scale. Finally, the random and alternate copolymers showed only one glass transition.

A. Dielectric Relaxations. A selected set of the dielectric loss curves as a function of frequency are presented in Figures 1, 2 and 3 for the samples A1, R2 and D2, respectively. The data correspond to temperatures above (a) and below (b) the glass transition region.

At high temperatures, the alternate copolymer A1 (see Fig. 1a) shows a conductive process (σ) that appears as a strong growth of the imaginary part of the permittivity at low frequencies. In this temperature range, the α relaxation overlaps the low frequency wing of the β process. A similar behaviour was observed for the random copolymers R1 (not shown), R2 (see Fig. 2a) and the disordered diblock sample D1 (not shown). On the other hand, the microsegregated diblock samples, D2 (see Fig. 3a) and D3 (not shown) do not show an explicit α peak in the glass transition region. The analysis of the dielectric loss curves has been made by fitting the experimental results to the equation:

$$\varepsilon''(\omega) = \left(\frac{\sigma}{\varepsilon_0 \omega}\right)^s + \sum_{k=\alpha,\beta} \mathrm{Im}\left\{\frac{\Delta\varepsilon_k}{\left[1+(\mathrm{i}\omega\tau_{HN,k})^{a_k}\right]^{b_k}}\right\}, \qquad (1)$$

where $\omega = 2\pi f$ is the angular frequency. The first term of the right hand side accounts for the ionic conductivity (σ), the deviation of the exponent $0 \le s \le 1$ from the unity (d.c. conductivity) represents the effect of blocking phenomena in the migration of charge carriers, and ε_0 is the dielectric permittivity of the vacuum. The sum describes the relaxation peaks, α and β, as Havriliak Negami (HN) model functions [31], $\Delta\varepsilon$ being the dielectric strength (i.e. the difference of the real part of the dielectric permittivity between the relaxed and unrelaxed state); τ_{HN} is the parametric relaxation time, and *a* and *b* ($0 \le a, ab \le 1$) are the shape exponents, related to the width and asymmetry of the relaxation. It has to be stressed that only when the σ, α and β contributions appeared at separate frequencies, all the parameters were allowed to be freely fitted. Even when the β relaxation peak is well defined (R2, D1, D2 and D3 samples), a complete HN function has been necessary to describe it; the asymmetric nature of the secondary relaxation is in agreement with the results found for the PMMA homopolymer [24]. When the segmental and secondary relaxations strongly overlap the determination of the shape

parameters becomes difficult. In this case, the α relaxation – right wing of the band (exponent b_α) and the β relaxation –left wing of the band (exponent a_β) were fixed to values extrapolated from low temperatures. Finally, it is essential to use the expression (1) to describe the loss curves of the samples D2 (see Fig. 3a) and D3, specially the minimum between the conductivity and the secondary process. However, in this case a symmetric α peak ($a_\alpha = b_\alpha$ with fixed value) gave satisfactory results.

In the sub T_g region, the A1 (Fig. 1b) and R1 (not shown) copolymers show two clear peaks, assigned to the β and γ relaxations, respectively; whereas R2 (see Fig. 2b), D1, D2 (Fig. 3b) and D3 show only a β peak. In the frequency domain the low temperature loss curves of A1 and R1 were analyzed in terms of the expression:

$$\varepsilon''(\omega) = \sum_{k=\beta,\gamma} \mathrm{Im}\left\{\frac{\Delta\varepsilon_k}{\left[1+(\mathrm{i}\omega\tau_{HN,k})^{a_k}\right]^{b_k}}\right\}, \qquad (2)$$

where now the HN functions describe the secondary β and γ processes. Both peaks were described using asymmetrical functions to ensure a good fitting quality, which is consistent with the asymmetric character of the β relaxation at high temperatures. However, when the overlapping is strong, the shape parameters b_β and a_γ were fixed to estimated values, obtained by means from a first free fitting. As it can be seen in the Fig. 2b a single HN function is not appropriate to describe the loss curves of the sample R2, underestimating the high frequency flank, whereas it is sufficient for the samples D1, D2 (Fig. 3b) and D3.

An alternative analysis of the R2 isotherms can be done in the time domain region, by transforming the complex permittivity to retardation spectra using a non linear regularization method [26, 32, 33]. We have fitted this set of spectra using a linear combination of two time-domain Havriliak Negami distributions, $L(\ln\tau) = \sum_{k=\beta,\gamma} \Delta\varepsilon_k L_k(\ln\tau)$ where:

$$L_k(\ln\tau) = \frac{1}{\pi}\frac{(\tau/\tau_{HN,k})^{a_k b_k}\sin(b_k\theta_k)}{[(\tau/\tau_{HN,k})^{2a_k} + 2(\tau/\tau_{HN,k})^{a_k}\cos(\pi a_k)+1]^{b_k/2}}, \qquad (3a)$$

with

$$\theta_k = \arctan\left[\frac{\sin(\pi a_k)}{(\tau/\tau_{HN,k})^{a_k} + \cos(\pi a_k)}\right], \tag{3b}$$

for $\theta > 0$. Otherwise if $\theta < 0$ then $\theta_k = \arctan\left[f_k(\tau_{HN,k}, a_k, b_k)\right] + \pi$, where $f_k(\tau_{HN,k}, a_k, b_k)$ is the argument of the trigonometric function in Eq. (3b) [34]. The $(\Delta\varepsilon_k, \tau_{HN,k}, a_k, b_k)$ parameters have the same meaning as in the frequency domain function, e.g. see Eqs. (1-2). The a_γ parameter was fixed to an estimated value from a first free fitting. For the sake of example, Figure 4 shows the results obtained by this procedure for the temperature 275 K and the existence of two sub T_g processes for the sample R2 is clearly visible.

Following the procedure described above, it was possible to fit all the frequency domain loss curves, and to build the relaxation map for the different relaxation processes. Figure 5 plots the temperature dependence of the dielectric relaxation strength for the samples A1, R2 and D2. It can be observed that the dielectric strength of the secondary relaxations increases slightly in the sub T_g region which is consistent with a thermally activated mechanism. The increasing rate of the β relaxation strength is higher above T_g due to the lower viscosity. On the other hand, the α relaxation strength for the samples A1 and R2 decreases, which is consistent with the free volume activation description of the α transition. The tendency of the α process strength of D2 is not clear because the contribution is hidden by the secondary relaxation. The rest of the samples show the following trend of the dielectric strengths: R1 ~ A1, D1 ~ D2 and D3 ~ D2 (results not shown). The values of the shape parameters of the secondary relaxations ($a_{\beta,\gamma} \approx$ 0.3-0.5, $b_{\beta,\gamma} \approx$ 0.4-0.6) are rather unusual and decrease with T (not shown). However for the segmental relaxation $a_\alpha \approx$ 0.5-0.9 and increases with T thus making the α process narrower; finally, $b_\alpha \approx$ 0.3 was almost constant. The mentioned trends are consistent with the interpretation of the HN exponents made by Schlosser & Schönhals [35]. Figure 6 shows the inverse temperature dependence of the characteristic retardation time, τ_{max}, corresponding to the frequency of the maximum of the loss peaks:

$$\tau_{\max} = \tau_{HN} \left\{ \frac{\sin\{[\pi ab]/[2(1+b)]\}}{\sin\{[ab]/[2(1+b)]\}} \right\}^{1/(1-a)}, \quad (4)$$

calculated from *a, b* and τ_{HN} parameters of the HN expression [35].

In general, the secondary relaxations (β and γ) exhibit Arrhenius behaviour,

$$\tau_{\max} = \tau_{0,Arr} \exp\left(\frac{E_A}{k_B T}\right), \quad (5)$$

where $\tau_{0,Arr}$ is a preexponential time, k_B the Boltzmann constant and E_A the activation energy. In the merging region with the α mode there are clear deviations of the activation energy for the β relaxation for the samples R2 (Fig. 6a) and D3 (Fig. 6b). The origin of the change in the slope can be attributed to a physical coupling of the relaxations [37], or to a methodological reason (statistical dependence of the relaxation functions [24, 38]). An alternative analysis of the R2 case will be carried out in the section III.B.

In the low temperature range, one of the most important facts is the existence of two secondary processes for the alternate (A1) and random (R1, R2) copolymers, but only one for the diblock samples (D1, D2, D3). The activation energy of the β process of the syndiotactic PMMA is 79 *kJ mol*$^{-1}$ [24], which is very similar to the values obtained for the diblock copolymers (see Table 2). However, for the A and R copolymers, $E_{A,\beta}$ differs from the value of the homopolymer, with values that may be correlated to the molar fraction of MMA groups in agreement with previous studies [39]. The samples A1 and R1, with almost the same MMA fraction (0.5 and 0.4, respectively), show the same activation energy of the β relaxation, 58 *kJ mol*$^{-1}$, smaller than the one for β mode of R2 (X_{MMA}=0.75) for which $E_{A,\beta}$=75 *kJ mol*$^{-1}$, a value close to that of PMMA; the preexponential times follow a similar pattern. The γ process seems to be more intense for samples A1 and R1 (with nearly equimolar quantities of MMA an S)

than for R2 (see Fig. 5). In the former DMTA study [21] the low time KWW contribution, presumably related to the secondary relaxations, showed higher activation energies than the β and the γ dielectric

processes for the homogeneous samples (A1, R1, R2 and D1), while they were lower for the microsegregated samples (D2 and D3).

The present experimental results do not allow to rigorously determine the molecular origin of the additional dielectric mode, γ, but it has to be related to the only polar group, the methylmethacrylate monomers. It might result from the incorporation of MMA groups in statistical copolymeric architectures which would provide different local environments for the dielectrically active group. The possibility that the γ relaxation is related to the styrene fraction is clearly improbable, due to its much weaker dielectric response. The β relaxation in the PMMA homopolymer has been attributed to the rotation of methacrylate group [19], therefore it might be possible to attribute the origin of the γ relaxation to the rotation of the MMA monomers in a local environment rich in styrene (S) monomers, while the β relaxation corresponds to the rotation of MMA in local environments rich in MMA groups. This idea is supported by the absence of γ modes in diblock samples where the MMA group is mostly surrounded by other MMA monomers. Further support to this idea is given by the fact that for the R2 sample, rich in MMA group, the intensity of the γ relaxation and the corresponding activation energy are smaller than for A1 and R1 (see Table 2). These results are in qualitative agreement with the results obtained by calorimetry [21]; in effect, the width of the glass transition regions for the PMMA block of the D2 and D3 samples are almost equal to that of the PMMA copolymer. Nevertheless, the Tg's of the PMMA blocks in D2 and D3 are clearly shifted to higher temperatures, and for R2 the width of the glass transition is almost twice that of the PS homopolymer. All these results are compatible with the fact that there may be differences in the local environment of the two monomers as discussed above. However, this seems to disagree with the DMTA results of Morais et al. [21] that indicate that there was no clear correlation between the MMA content of the polymer and the T_g for the homogeneous samples (A1, R1, R2, and D1).

The temperature dependence of the α relaxation can be described by a VFT equation:

$$\tau_{\max} = \tau_{0,VFT} \exp\left(\frac{DT_V}{T - T_V}\right), \quad (6)$$

where $\tau_{0,VFT}$ is a preexponential time, D is the strength parameter which measures the deviation from the Arrhenius behaviour, and T_V the Vogel temperature or ideal glass transition. For the subset of disordered samples (A1, R1, R2 and D1), with only one T_g, the dynamic glass transition is described with the following parameters (see Table 2): $T_V \approx 320\ K$ and $D \approx$ 5-6, which reveal the relatively fragile character of these copolymers ($D < 10$) [40]. The only significant difference becomes from the parameter $\tau_{0,VFT} \approx 10^{-13}$-$10^{-11}\ s$. These results suggest that, despite the cooperative nature of α relaxation, for the copolymers studied it does not depend strongly on macroscopic features such as molecular architecture or relative composition of polar groups (MMA). Diblock copolymers D2 and D3, due to their microsegregated nature, are expected to present values of T_g close to that of PMMA, although it has been reported that $\tau_{0,VFT} \approx 10^{-11}\ s$, $T_V = 381\ K$, and $D = 2$ for syndiotactic homopolymer [24, that are rather different from the values of the D2 and D3 samples, even considering the T_g differences. The most likely cause of this discrepancy is that in the D2 and D3 samples the α mode has been described by a symmetric Cole-Cole peak, whereas the dynamic glass transition is strongly asymmetric in the case of PMMA. The accurate prediction of the shape of the α mode in the present samples is strongly complicated by the overlapping with a conductive process influenced by the interface blocking effects, with exponents far from unity ($s \approx 0.7$). Its relatively high intensity at moderate frequencies hides completely the α peak (see Fig. 3a), thus complicating the analysis of the data. In contrast for a disordered PMMA sample the conductivity is purely ohmic ($s \approx 1$) and the overlapping with dielectric processes is not critical. Therefore, in the context of the description made here, the α contribution to the dielectric loss of D2 and D3 accounts for the influence of the dynamic glass transition in the β relaxation through which virtually all the polarization relaxes.

B. Merging of the α and β Relaxations in the R2 sample. In the previous section we have used the classical additive approach to describe the experimental data, i.e. the relaxation peaks were fitted to a sum of HN empirical functions, given by Equation (1), this method will be denoted as SHN hereinafter. According to this, the activation energy of the β relaxation seems to be higher when it merges with the α relaxation as clearly observed for R2 sample (see Fig. 6). In order to study the merging of the relaxations for R2 an alternative analysis has been developed which is based on the *Williams Ansatz*, thus implying that the α and β relaxations are statistically independent processes [27]. When only autocorrelation terms are considered, a simplified version of the *ansatz* states that the whole relaxation function in the time domain is given by:

$$\phi(t) = \phi_\alpha(t)[f_\alpha + (1-f_\alpha)\phi_\beta(t)], \tag{7}$$

where $\phi_\alpha(t)$ and $\phi_\beta(t)$ are the relaxation functions of the α and β processes, respectively, and $(1-f_\alpha)$ takes into account the partial relaxation through the mechanisms involved in the β process. When both modes decay at very different time scales the Eq. (7) reduces to a sum of relaxation functions and, hence the SHN method is appropriate.

The starting point has been to calculate the relaxation function, $\phi_{\exp}(t)$ from the frequency domain results making use of the retardation spectra, $L(\ln\tau)$ in terms of mono-exponential relaxations:

$$\phi(t) = N^{-1}\int_{-\infty}^{\infty} L(\ln\tau)e^{-t/\tau}d\ln\tau, \tag{8}$$

where the constant N and the 'experimental' spectra $L(\ln\tau)$ were obtained from the complex permittivity, $\varepsilon^*(\omega)$, by means of the method described in the Reference [26]. The algorithm used implements the Tikhonov regularization method with a kernel that, besides the relaxational integral term, includes a conductivity contribution analogous to the σ term of Eq. (1). The spectra were calculated two decades above and below the experimental frequency window in order to avoid spurious contributions near the integration limits. Following this approach the retardation spectra for the high

temperature isotherms of the R2 sample (Fig. 2a) were obtained, and some of them are shown in the inset of the Fig. 7. The normalized relaxation functions of the Fig. 7 were calculated using Eq. (8) with $N = \int_{-\infty}^{\infty} L(\ln\tau) d\ln\tau$ and, in this case it can be shown that $N = \Delta\varepsilon$, the total dielectric strength.

The second step is to choose an adequate expression of the *Williams Ansatz*, or Eq. (7). In previous studies of homopolymer systems [24-25] a Kohlrausch-Williams-Watts function was used to describe the α contribution, $\phi_\alpha(t)$. However, for multi-component systems, like copolymers, the concentration fluctuations broaden the dynamic glass transition and a single KWW function may fail in fitting the α relaxation [41]. Concerning the β relaxation the KWW function is a good candidate but it lacks information about the asymmetry of the process, i. e. the *b* exponent contained in the HN function; which is a problem because in the present case the β process has revealed to be notably asymmetrical. Therefore, we have used the same functional dependency used in the frequency domain additive approach (SHN) for $\phi_\alpha(t)$ and $\phi_\beta(t)$. After combining the *Williams Ansatz*, the HN distributions and Eqs. (7) and (8) the relaxation function can be written as:

$$\begin{aligned}\phi_{WA}(t) = f_\alpha N_\alpha^{-1}\int_{-\infty}^{\infty} L_\alpha(\ln\tau;\tau_{HN,\alpha},a_\alpha,b_\alpha)e^{-t/\tau}d\ln\tau + \\ +(1-f_\alpha)N_\alpha^{-1}N_\beta^{-1}\int_{-\infty}^{\infty}\int_{-\infty}^{\infty} L_\alpha(\ln\tau;\tau_{HN,\alpha},a_\alpha,b_\alpha)L_\alpha(\ln\tau';\tau_{HN,\beta},a_\beta,b_\beta)e^{-t(1/\tau+1/\tau')}d\ln\tau d\ln\tau'\end{aligned}, \quad (9)$$

where $L_k(\ln\tau;\tau_{HN,k},a_k,b_k)$ are the HN distributions defined as in Eq. (3) for $k=\alpha, \beta$ processes and N_k are normalizing constants.

Once the experimental relaxation functions, $\phi_{\exp}(t_j)$, have been calculated in a set of points $t_j, j = 1,...,m$; the problem is to solve the quadratic minimization:

$$\min_S\left[\sum_{j=1}^{m}|\phi_{\exp}(t_j)-\phi_{WA}(t_j)|^2\right], \quad (10)$$

where $\phi_{WA}(t)$ is given by Eq. (9). The minimization is made for the general parameter set $S \equiv (f_\alpha, N_k, \tau_{HN,k}, a_k, b_k)$ with $k = \alpha,\beta$. This approach, denoted in the following as WAHN, has been

implemented using commercial software (MATLAB 7.6, The MathWorks Inc., Natick, MA, 2000). First, the integrals are solved numerically by the composite Boole's rule and then a sequential quadratic programming algorithm is used to carry out the optimization.

As long as the experimental relaxation functions $\phi_{\exp}(t_j)$ are normalized, the terms $\phi_\alpha(t)$ and $\phi_\beta(t)$ of the model function $\phi_{WA}(t)$ can be also considered as normalized. That is, if $N = \int_{-\infty}^{\infty} L(\ln\tau) d\ln\tau$ is used in Eq. (7) then the partial constants are $N_k = 1$. The WAHN method has been applied for the normalized relaxation functions of R2 (Fig. 7) considering that the time scale values of the β process follows the low temperature extrapolated trend. That is, a non linear restriction given by the Eq. (4) has been introduced for the reduced parameter set $S' \equiv (f_\alpha, \tau_{HN,k}, a_k, b_k)$, where the $\tau_{\max}(\beta)$ values have been extrapolated from the Arrhenius behaviour at $T<T_g$. This constraint reduces the number of degrees of freedom to six, the same free parameters used in the fitting procedure to a sum of HN functions in the frequency domain (SHN). The results of the WAHN method in the normalized case are shown in Fig. 7, where the $\phi_{WA}(t)$ fits describe satisfactorily the $\phi_{\exp}(t)$ experimental curves. The set S' of optimized parameters can be directly compared to the parameter values resulting from the SHN method. The time scales of the α relaxation in the WAHN framework were calculated through Eq. (4), and, as noted before, the values of the β relaxation time were fixed. As can be seen in Fig. 8 the differences in the $\tau_{\max}(\alpha)$ values comparing both methods are not systematic and might be attributed to the errors derived from the numerical determination of the time domain relaxation functions. It can be stated that the time scale of the α relaxation are the same in both approaches within their uncertainties. Furthermore, for the WAHN method, the extrapolation of the β relaxation times from low temperature behavior did not affect to the α relaxation times. Figure 9 shows the HN exponents derived from both approaches: for the SHN method, for T > 400 K, the b exponent of the α mode have been fixed to a mean value, $b_\alpha = 0.24$, and the strong overlapping with the β process does not allow describing the right wing band of the α peak. For the WAHN method b_α fluctuates around $b_\alpha = 0.3$, which is not far from the value

obtained by SHN. On the other hand, the a_α exponent from the SHN method increases with *T*, while the WAHN analysis predicts a nearly constant value, $a_\alpha = 0.6$. The shape exponents of the β mode derived from the SHN analysis does not follow the low temperature trends when both modes overlap but show anomalous oscillations. When the WAHN method is used the b_β parameter follows the sub T_g tendency while the a_β parameter does not, which may be due to a real change of the shape of the β relaxation when it overlaps with the α mode.

The relaxation function in the frequency domain is defined as $\Phi^*(\omega) = (\varepsilon^*(\omega) - \varepsilon_\infty)/N$, where ε_∞ is the high frequency limit of the permittivity and N is a constant. This function is related to the time domain response through $\Phi^*(\omega) = \mathbf{L}_{i\omega}\left[-\dot{\phi}(t)\right]$, where $\mathbf{L}_{i\omega}$ is the Laplace transform with the imaginary exponent $i\omega$, and $\dot{\Phi} = d\Phi/dt$. Therefore, the transformation of the WAHN equation (9) into the frequency domain yields:

$$\Phi^*(\omega) = f_\alpha N_\alpha^{-1}\Phi_\alpha^* - (1-f_\alpha)N_\alpha^{-1}N_\beta^{-1}\Phi_{\beta eff}^*(\omega), \tag{11a}$$

where the term related to the α relaxation can be expressed as

$$\Phi_\alpha^*(\omega) = 1 - i\omega\mathbf{L}_{i\omega}\left[\int_{-\infty}^{\infty} L_\alpha(\ln\tau;\tau_{HN,\alpha},a_\alpha,b_\alpha)e^{-t/\tau}d\ln\tau\right], \tag{11b}$$

using the property $\mathbf{L}_z\left[\dot{f}\right] = 1 - z\mathbf{L}_z[f]$, and the β *effective* relaxation have been defined as $\Phi_{\beta eff}^*(\omega) = \mathbf{L}_{i\omega}\left[-d(\phi_\alpha\phi_\beta)/dt\right]$ and can be expressed as [25]:

$$\Phi_{\beta eff}^*(\omega) = \int_{-\infty}^{\infty} L_\alpha(\ln\tau;\tau_{HN,\alpha},a_\alpha,b_\alpha)\left[\int_{-\infty}^{\infty}\frac{L_\beta(\ln\tau;\tau_{HN,\beta},a_\beta,b_\beta)}{1+i\omega\left(\tau^{-1}+\tau'^{-1}\right)^{-1}}d\ln\tau'\right]d\ln\tau\,. \tag{11c}$$

In the normalized case $N = \Delta\varepsilon$ and $N_k = 1$. The β *effective* process, from the $\phi_\alpha\phi_\beta$ term in the *Williams Ansatz* must be understood as the partial β relaxation in the fixed environment given by the α mechanism. In practice, this effective mode represents the link between both methods. Comparing the relaxational terms of Eq. (1) with Eq. (11a) the β *effective* relaxation of the WAHN approach is related

to the β relaxation of the classical SHN approach. The apparent change of molecular mechanisms responsible of the β process in the additive approach is solved in the Williams Ansatz framework through the presence of a β *effective* process, originated from the statistical independence of the relaxations.

In the non normalized scheme the frequency domain relaxation function is $\Phi^*(\omega) = \varepsilon^*(\omega) - \varepsilon_\infty$ and their imaginary part is the dielectric loss. In this case the N_k parameters are non trivial and comparing again Eq. (11) to Eq. (1) the following identification can be made (SHN $\leftrightarrow$ WAHN):

$$\Delta\varepsilon_\alpha \leftrightarrow f_\alpha N_\alpha^{-1} \quad ; \quad \Delta\varepsilon_\beta \leftrightarrow (1-f_\alpha) N_\alpha^{-1} N_\beta^{-1}. \tag{12}$$

In order to get these intensities the WAHN method has been applied to the non normalized relaxation functions of R2, i. e. the $\phi_{\exp}(t_j)$ were calculated through Eq. (8) with $N = 1$. The full set $S \equiv (f_\alpha, N_k, \tau_{HN,k}, a_k, b_k)$ must be taken into account but the subset $S' \equiv (f_\alpha, \tau_{HN,k}, a_k, b_k)$ has been fixed to the values obtained in the previous normalized analysis. Only the N_k constants have been optimized. To check the validity of the procedure, instead of showing the non normalized time domain relaxation functions the optimized parameters have been used to numerically integrate the Eq. (11) and hence to complete the transformation to the frequency domain. The results are shown in the Fig. 10 compared to the experimental dielectric loss curves, to which the conductivity contributions from the SHN analysis have been subtracted. The overall quality of the fittings is not as good as in the normalized case (see Fig. 7), so the determination of the N_k constants is compromised by the goodness of fit in this case. On the other hand the optimized $(f_\alpha, \tau_{HN,k}, a_k, b_k)$ parameters are related to the better goodness of fit of the normalized analysis. Anyway, the maximum of the β (*effective*) peak are well described, validating the constraint in $\tau_{\max}(\beta)$ values extrapolated from low temperatures. There is an important deviation for the lowest temperature around the α peak, possibly due to the introduced error when subtracting the conductivity. Also for the highest temperature curve the fit is poor because the β peak is almost outside the window and, in addition a strong overlapping exists. Concerning the

dielectric strength information, the assignations made in Eq. (12) should be considered indeed as equalities, and Fig. 11 shows that the WAHN parameter combination describe very well the trends of the dielectric strengths obtained from the SHN method.

C. Molecular Dynamic Simulation of the Secondary Relaxations. In a simplified picture, where the intermolecular correlations are neglected and assuming a high dielectric strength, the macroscopic relaxation function can be directly identified with a microscopic magnitude given by the molecular dipole time-correlation function [36]. The time-correlation function *A(t)* of the orientation of the ester bond vector C=O, $\mathbf{b}_{C=O}$, allows us to calculate the characteristic relaxation time of the nearly antiparallel ester group dipole moment that can be related to the experimental magnitudes for the β relaxations. Therefore, $A(t)$ has been fitted to the a sum of KWW exponentials:

$$A(t) \equiv \left\langle \mathbf{b}_{C=O}(\tau) \cdot \mathbf{b}_{C=O}(\tau + t) \right\rangle \Big/ \left\langle \mathbf{b}^2_{C=O}(\tau) \right\rangle = \sum_i A_i \exp\left[-\left(t / \tau_i \right)^{\beta_i} \right]. \qquad (13)$$

Parameters A_i, τ_i and β_i are obtained by means of a direct non-linear fitting procedure, considering one or two stretched exponentials; the results for the PMMA chains can be satisfactorily fitted to a single exponential. This is illustrated in the inset of the Figure 12, where *ln[A(t)]* vs. t^{β} is shown, with the customary β=0.5 value for PMMA and for the alternate copolymer at 600 *K*. It can be observed that the PMMA chain has a single exponential behaviour, while for the alternate copolymer a fit to two exponentials is clearly required, which agrees with the more complex secondary relaxation of observed in the analysis of our experiments for the copolymers.

The final numerical fits are actually carried out by considering a free variation of parameters τ_1 and β_1. The fits for the alternate chains are performed by fixing the exponent value for longer times, β_2, to be the same obtained for PMMA systems at the same temperature (except for the T=500 *K*, case that requires a higher value) while the rest of parameters (coefficients, relaxation times and β_1) are freely varied.

The described fitting procedures are satisfactorily used for the systems at different temperatures. (See for example Figure 12). It should be remarked that most values of the β_i are in the range 0.4-0.6, while the A_i coefficients for the two exponential fits are always close to the 0.5 values. The ratios between values corresponding to the first and second relaxation time in any given alternate chain system are similar to those found in our analysis of the experimental data.

The activation energies for the two types of systems can be calculated from the Arrhenius fits of the τ_{mean} values that depend on τ, and β (see Figure 13 and Eq. (5)). The value obtained for the PMMA systems, $E_A = 48\ kJ\ mol^{-1}$ is significantly higher than the results obtained for the alternate copolymers, $E_A = 23\ kJ\ mol^{-1}$ for the slower mode and $E_A = 16\ kJ\ mol^{-1}$ for the faster mode. The experimental data show also higher activation energy for the slower mode. Although the values predicted from the experimental relaxations are generally higher (see Table 2), the experimental and simulation results for the activation energies are relatively close, considering the great influence that some details in the molecular model (such as the forcefield parameters) may have on the final simulation results.

IV. Conclusions

Dielectric relaxation experiments of six styrene-co-methyl methacrylate (MMA) copolymers with different architectures (random, alternate and diblock) haven been carried out over the $193 \leq T / K \leq 423$ and $0.01 \leq f / \text{Hz} \leq 10^6$ ranges. Two of the diblock copolymers are microsegregated, while the other four copolymers present a homogeneous phase.

The ε" vs. f curves clearly show two differentiated sub-T_g relaxations for the alternate and the styrene-richest random copolymers, while for the rest only one β process can be distinguished. The analysis of the data in both the frequency and time domains indicate that to describe the sub-T_g transitions within the experimental precision two asymmetric Havriliak-Negami functions have to be used (corresponding to the β and γ relaxations for the alternate and the random copolymers). However,

only one β relaxation seems to exist within the experimental window for the three block copolymers and the PMMA homopolymer.

The relaxation times of the α-relaxation present a VFT temperature dependence, while the sub-T_g transitions follow an Arrhenius dependence. The activation energy, E_A, of the β relaxations for the diblock- and the MMA-rich random copolymers are very close to that of the PMMA homopolymer, while for the alternate and the styrene-rich random copolymer a lower E_A value is obtained. It is suggested that the origin of the γ-relaxation might be the rotation of the MMA groups in a styrene-rich environment.

An alternative analysis to the classical additive approach has been applied to the α and β merging relaxations of the R2 sample. This method is based on the simplified *Williams Ansatz* developed in terms of Havriliak Negami distributions. This framework postulates the existence of an effective β process originated from the intersection of statistical independent α and β modes. This effective mode is responsible of the apparent change of activation energy of the β relaxation in the merging region, from the classical additive point of view. Nevertheless, the deviations on the low temperature trends of the relaxation shape parameters are only partially corrected. A consistency test consisting of a frequency domain transformation has been developed, and it reproduces the dielectric strengths trend of the additive analysis.

Finally, the Molecular Dynamics simulations of PMMA and an alternate copolymer are in a relatively good qualitative agreement with the low temperature experimental results, although the predicted values for E_A for the simulations are smaller than the experimental values.

Acknowledgements

This work was supported in part by MICINN under grants FIS2009-14008-C02-01, MAT-2009-11083 and CTQ2010-16414, by CAM under grant P2009/ESP-1691, by ESA under grants FASES and PASTA, and by EU under grant Marie Curie ITN-MULTIFLOW. M. E. was supported by MICINN through a Ph.D. fellowship.

References

[1] D.R. Paul, C.B. Bucknall, eds, *Polymer Blends*, vol. 1 (New York, Wiley, 2000).

[2] I.W. Hamley, *The Physics of Block Copolymers* (Oxford, Oxford University Press, 1998).

[3] J.M.G. Cowie, *Polymers: Chemistry and Physics of Modern Materials*, 2nd edition (London, Chapman and Hall, 1991).

[4] T. Kokata, K. Adachi, Macromol Symp **3,** 124 (1997).

[5] I. Alig, F. Kremer, G. Fytas, J. Roovers, Macromolecules **25**, 5277 (1992).

[6] K. Karatasos, S.H. Anastasiadis, G. Floudas, G. Fytas, S. Pispas, H. Hadjichristidis, T. Pakula, Macromolecules **29**, 1326 (1996).

[7] A. Kyritsis, P. Pisis, S-M. Mai , C. Booth, Macromolecules **33**, 4581 (2000).

[8] S. Moreno, R.G. Rubio, Macromolecules **35**, 5483 (2002).

[9] L. Ma, Ch. He, T. Suzuki, M. Azuma, Y. Bin, H. Kurosu, M. Matsuo, Macromolecules **36**, 8056 (2003).

[10] M. Encinar, E. Guzmán, M.G. Prolongo, R.G. Rubio, C. Sandoval, F. Gonzalez-Nilo, L. Gargallo, D. Radic, Polymer **49**, 168 (2008).

[11] A. Zetsche, E.W. Fischer, Acta Polym **45**, 168 (1994).

[12] A-V.G. Ruzette, P. Banerjee, A.M. Mayes, M. Pollard, T.P. Russell, R. Jerome, S.R. Hjelm, P. Thiyarajan, Macromolecules **31**, 8509 (1998).

[13] T.P. Russell, R.P. Hjelm, P.A. Seeger, Macromolecules **23**, 890 (1990).

[14] T.E. Karis, T.P. Russell, Y. Gallot, A.M. Mayes, Macromolecules **28**, 1129 (1995).

[15] H. Ahn, D.Y. Ryu, Y. Kim, K.W. Kwon, J. Lee, J. Cho, Macromolecules **42**, 7897 (2009).

[16] V. Lupascu, S.J. Picken, M. Wubbenhorst, J Non-Cryst Solids **352**, 5594 (2006).

[17] R. Bergman, F. Alvarez, A. Alegría, J. Colmenero, J Non-Cryst Solids **235-238**, 580 (1998).

[18] A. Arbe, A-C. Genix, J. Colmenero, D. Richter, P. Fouquet, Soft Matter **4**, 1792 (2008).

[19] K. Schmidt-Rohr, A.S. Kulik, H.W. Beckhan, A. Ohlemacher, U Pawelzik, C. Boeffel, H.W. Spiess, Macromolecules **27**, 4733 (1994).

[20] J.F. de Dens, G.P. Souza, W.A. Corradini, T.D.Z. Atvars, L. Akcelrud, Macromolecules **38**, 6938 (2004).

[21] V. Morais, M. Encinar, M.G. Prolongo, R.G. Rubio, Polymer **47**, 2349 (2006).

[22] T. Pakula, G. Floudas. In: F. Baltá-Calleja, Z. Roslaniec, editors, *Block Copolymers* (New York, Marcel Decker, 2000).

[23] S. Theobald, W. Pechold, B. Stoll, Polymer **42**, 289 (2001).

[24] R. Bergman, F. Alvarez, A. Alegría, J. Colmenero, J Chem Phys **109**, 7546 (1998).

[25] D. Gómez, A. Alegría, A. Arbe, J. Colmenero, Macromolecules **34**, 503 (2001).

[26] G. Domínguez-Espinosa, D. Ginestar, M.J. Sanchís, R. Díaz Calleja, E. Riande, J Chem Phys **129**, 104513 (2008).

[27] G. Williams, C.D. Watts. In: P. Diehl, E. Fluck, H. Gunther, J.B. Robert, editors, *NMR. Basic Principles and Progress*, vol. 4 (Berlin, Springer-Verlag, 1971).

[28] M.G. Prolongo, C. Salom, R.M. Masegosa, S. Moreno, R.G. Rubio, Polymer **38**, 5097 (1997).

[29] H. Sun, S.J. Mumby, J.R. Maple, A.T. Hagler, J Am Chem Soc **116**, 2978 (1994).

[30] E. Saiz, J.P. Hummel, P.J. Flory, M. Plavsic, J Phys Chem **85**, 3211 (1981).

[31] S. Havriliak Jr, S.J. Havriliak, *Dielectric and Mechanical Relaxation in Materials: Analysis, Interpretation, and Application to Polymers,* chapter 1 (New York, Hanser Verlag, 1997).

[32] J. Weese, Comput Phys Commun **77,** 429 (1993).

[33] S. Moreno, R.G. Rubio, G. Luengo, F. Ortega, M.G. Prolongo, Eur Phys J E **4,** 173 (2001).

[34] R. Zorn R, J Polym Sci, Polym Phys B **38,** 1043 (1999).

[35] E. Schlosser, A. Schönhals, Colloid Polym Sci **267**, 963 (1989).

[36] E. Riande, R. Díaz-Calleja, *Electrical Properties of Polymers*, chapter 4 (New York, Marcel Dekker, 2004).

[38] K.L. Ngai, M. Paluch, J Chem Phys 120, 857 (2004).

[38] D. Gómez, A. Alegría, A. Arbe, J. Colmenero, Macromolecules **34**, 503 (2001).

[39] S. Mashimo, S. Yagihara, Y. Iwasa, J Polym Sci, Polym Phys Ed **16**, 1761 (1978).

[40] C.A. Angell, Science **267**, 1924 (1995).

[41] K.L. Ngai, Macromolecules, **32,** 7140 (1999).

Table 1. Characteristics of the different polymer samples

Sample	M_w *(kDa)*	M_w / M_n	M_w *(PS)(kDa)*	M_w *(PMMA) (kDa)*	*Type*	X_{MMA}
A1	382	1.49	-	-	Alternate	0.50
R1	71.3	1.86	-	-	Random	0.40
R2	305	1.83	-	-	Random	0.75
D1	179.3	1.04	172	7.3	Diblock	0.04
D2	547.1	1.05	154.8	392.3	Diblock	0.73
D3	503	1.10	253	250	Diblock	0.51

M_w is the weight average molecular weight, M_w/M_n is the polydispersity index, and X_{MMA} is the mole fraction of methylmethacrylate groups.

Table 2. Fitting parameters for the temperature dependence of the characteristic retardation time for the α [Eq. (6)] and β, γ [Eq. (5)] modes for all the copolymers. Abbrev. [DS]: Dielectric Spectroscopy experimental results. [MDS]: Molecular Dynamics Simulation results.

	A1	*R1*	*R2*	*D1*	*D2*	*D3*	*PMMA*
			α relaxation [DS]				Ref [24]
log $\tau_{0,VFT}$ (±0.5)	-11.1	-13.6	-10.5	-12.9	-10.9	-11.2	-10.8
D (±0.5)	4.4	6.2	4.7	5.1	9.7	14.7	2.3
T_V (±2 K)	322	318	316	324	274	232	370
			β relaxation [DS]				
log $\tau_{0,\beta}$ (±0.3)	-14.4	-14.4	-15.4	-15.8	-15.7	-15.6	-15.3
$E_{A,\beta}$ (±0.5 $kJ\ mol^{-1}$)	58.0	57.8	75.1	77.0	80.8	79.0	79.4
			γ relaxation [DS]				
log $\tau_{0,\gamma}$ (±0.6)[a]	-16.4	-14.0	-12.5	-	-	-	-
$E_{A,\gamma}$ (±0.5 $kJ\ mol^{-1}$)[a]	54.8	44.0	38.0	-	-	-	-
	Alternate chains			*Homopolymeric chains*			
			Slower contribution [MDS]				
log τ_0 (±0.4)	-11.1			-13.4			
E_A (±1 $kJ\ mol^{-1}$)	23			48			
			Faster contribution [MDS]				
log τ_0 (±0.4)	-11.7			-			
E_A (±0.5 $kJ\ mol^{-1}$)	16			-			

[a] The uncertainties for the sample R1 are: log $\tau_{0,\gamma}$ (±1) ; $E_{A,\gamma}$ (±2 $kJ\ mol^{-1}$)

Legends for the Figures

Figure 1. Selected isotherms of the imaginary part of the dielectric permittivity as a function of the frequency for the sample A1 in two regions: **(a)** near and above T_g, showing the segmental process, α, secondary relaxations, β and the conductivity, σ; and **(b)** below T_g, where the two secondary processes, β and γ, are present. The dotted lines correspond to the different contributions, σ, α, β and γ of the fitting (continuous line) following the Eq. (1) for the example isotherm at 399 K, and the Eq. (2) for the temperature 259 K. **Note**: In Fig. 1b the y-scale of the γ contribution is related to the right axis, while the left axis is used for the rest of the curves.

Figure 2. Selected isotherms of the imaginary part of the dielectric permittivity as a function of the frequency for the sample R2 at temperatures **(a)** near and above T_g, showing the segmental process, α, secondary relaxations, β and the conductivity, σ. Here, the dotted lines correspond to the different contributions of the fitting (continuous line) in the Eq. (1), σ, α and β for the example isotherm 391 K. Figure **(b)** correspond to isotherms below the glass transition, where a main sub-T_g relaxation, β, is not completely described with only one HN model function (dotted curves for the isotherms 243 K and 259 K).

Figure 3. Selected isotherms of the imaginary part of the dielectric permittivity as a function of the frequency for the sample D1 in two regions: **(a)** near and above T_g, where a dominant β relaxation and a conductive process, σ, are present. Here, the dotted lines correspond to the different contributions of the fitting (continuous line) in the Eq. (1), σ and β and also a contribution related to the hidden α relaxation for the example isotherm 415 K. Figure **(b)** represents selected loss curves below T_g, where the β peak is described with only one HN model function (dotted curve) as it can be seen for the 275 K and 307 K isotherms.

Figure 4. Retardation time spectra corresponding to the 275 K isotherm of the dielectric permittivity of the sample R2. The line is a fitting to a sum of two HN contributions (dotted lines), one describing the high time (low frequency) β process and another one at low times (high frequencies) corresponding to the weak γ relaxation.

Figure 5. Temperature dependency of the dielectric strength for the different dynamic processes of the samples A1, R2 and D2. The error bars, when not explicitly drawn, are smaller than the size of the symbols

Figure 6. Relaxation maps for the samples: **(a)** A1, R1 and R2; **(b)** D1, D2 and D3 as stated in the legends. The error bars, when not explicitly drawn, are smaller than the size of the symbols. The continuous lines are Arrhenius fits, Eq. (5) for the secondary relaxations, and VFT fits, Eq. (6), for the α relaxation. The dashed lines are the α and β relaxation tendencies for the syndiotactic PMMA (taken from the reference [24]).

Figure 7. Normalized time domain relaxation functions calculated from the experimental results (symbols). The different curves correspond to the temperatures from right to left: 389, 397, 409, 419, 429 and 435 K. The continuous lines are the fittings to the WAHN model described by the equations (9-10). The vertical dashed line delimitates the high frequency limit of the experimental window. Inset: Retardation time spectra obtained from the complex permittivity for selected temperatures.

Figure 8. Relaxation map at $T>T_g$ for R2 copolymer. The relaxation times are calculated by means of Eq. (4) using the parameter values obtained from the SHN method (closed symbols, Eq. (1)) and, alternatively, from the WAHN method in the time domain (open symbols, Eqs. (9-10). The time scale of the β process in the WAHN approach is extrapolated from the sub T_g Arrhenius trend (continuous line).

Figure 9. Havriliak- Negami shape parameters for the α and β processes of the R2 copolymer obtained from the SHN method (closed symbols, Eq. (1)) and, alternatively, from the WAHN method (open symbols, Eqs. (9-10)). The line represents the extrapolation of the sub T_g trend of the *a* and *b* parameters of the β mode. Some representative error bars are drawn.

Figure 10. Experimental dielectric loss curves without the conductivity contribution of the R2 sample (symbols). The continuous lines are the fittings according the WAHN method (minimization: Eq. (10); and frequency domain transformation: Eq. (11)). The different curves correspond to the temperatures from right to left: 389, 397, 409, 419, 429 and 435 K.

Figure 11. Temperature dependency of the dielectric strengths for the α and β processes of the R2 copolymer obtained from the SHN method (closed symbols, Eq. (1)). They are compared to the magnitudes for the α and β_{eff} processes from the WAHN method (open symbols, Eqs. (9-11)) by means of the Eq. (12).

Figure 12. Direct fitting (continuous lines) of the correlation functions for the PMMA and alternate chains at 600K to the Eq. (13) (only one KWW is used in the homopolymer case). Inset: logarithmic plot of the correlation functions. The abscissa is the time (in picoseconds) elevated to the stretching exponent, chosen as 0.5.

Figure 13. Arrhenius plots of the KWW mean relaxation times for the two alternate modes and the PMMA mode.

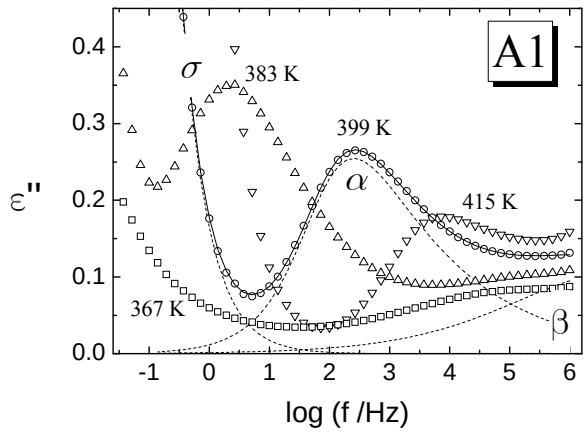

Figure 1a.

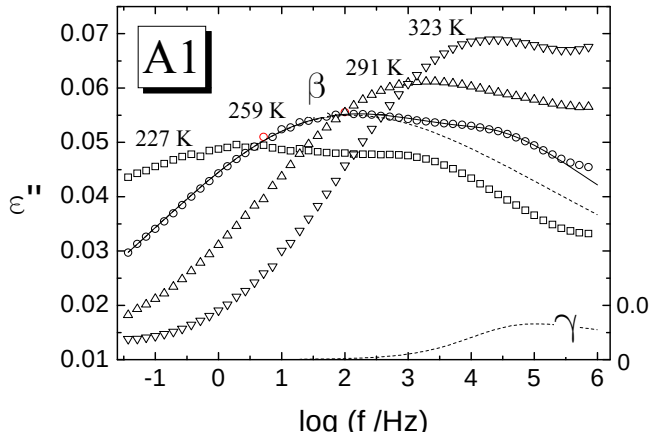

Figure 1b.

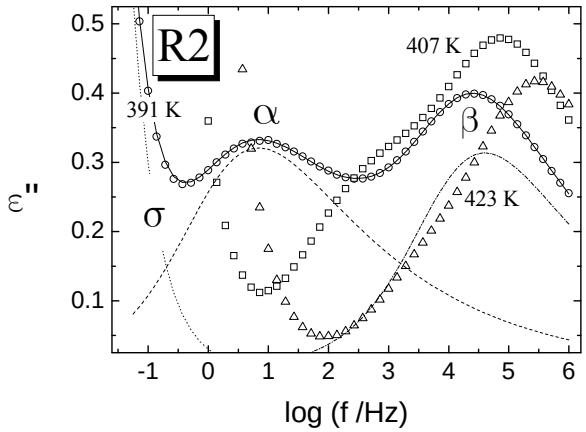

Figure 2a.

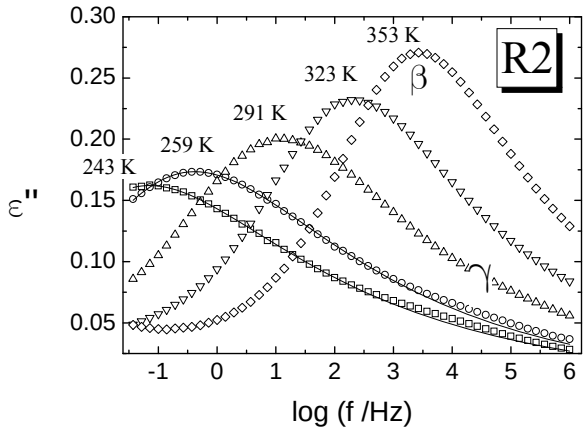

Figure 2b.

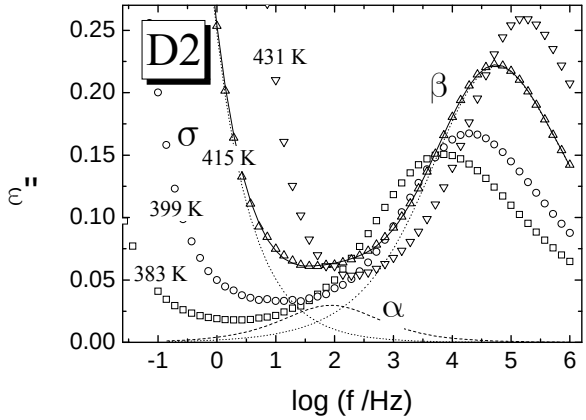

Figure 3a.

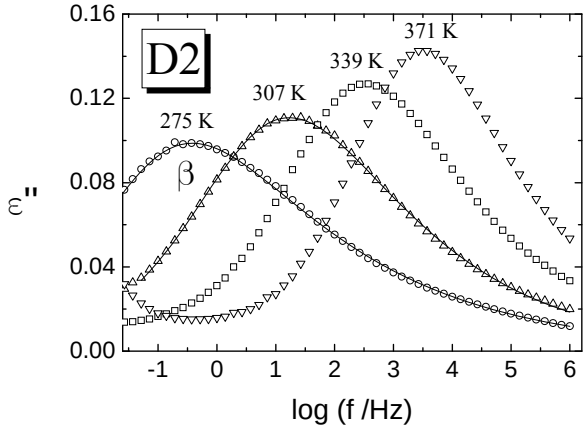

Figure 3b.

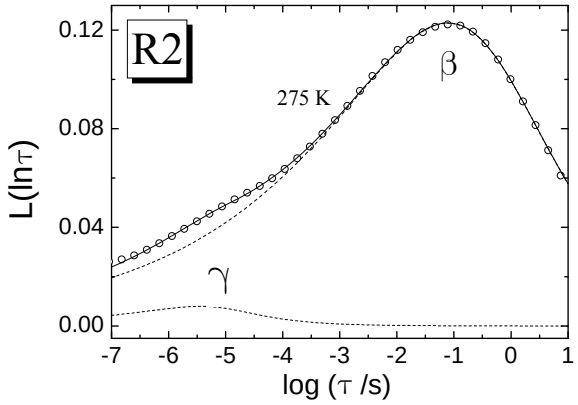

Figure 4.

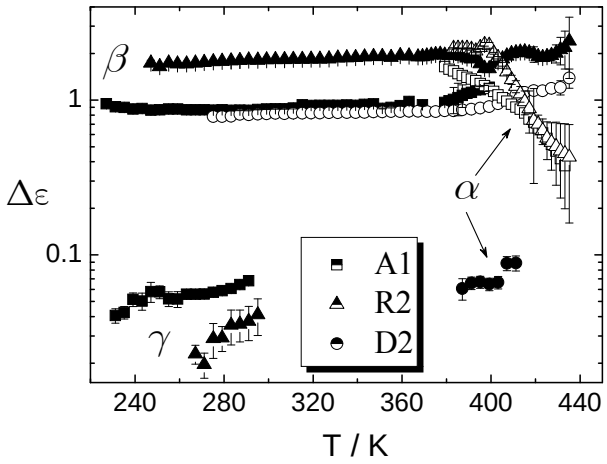

Figure 5.

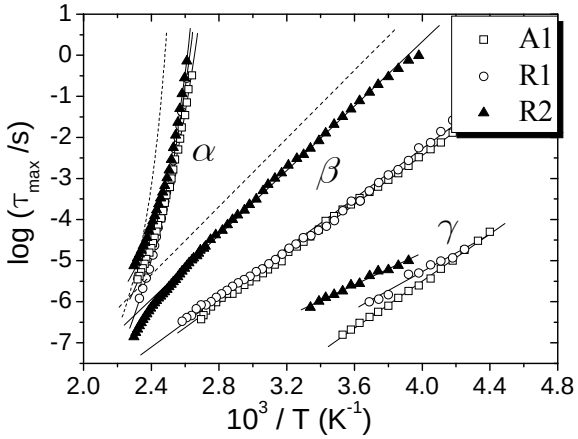

Figure 6a.

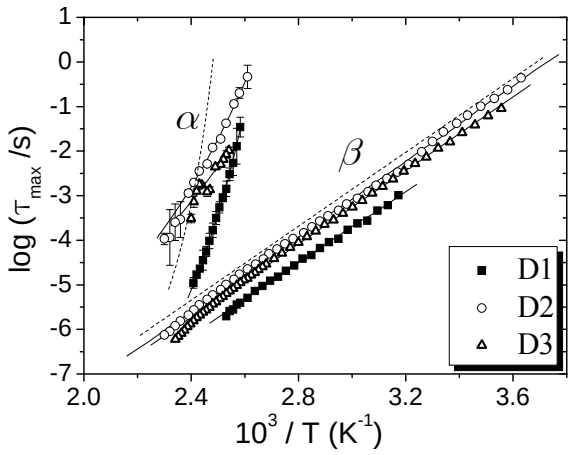

Figure 6b.

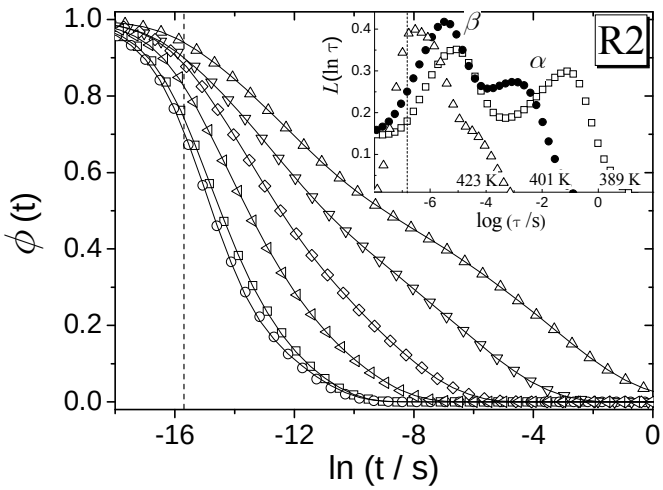

Figure 7.

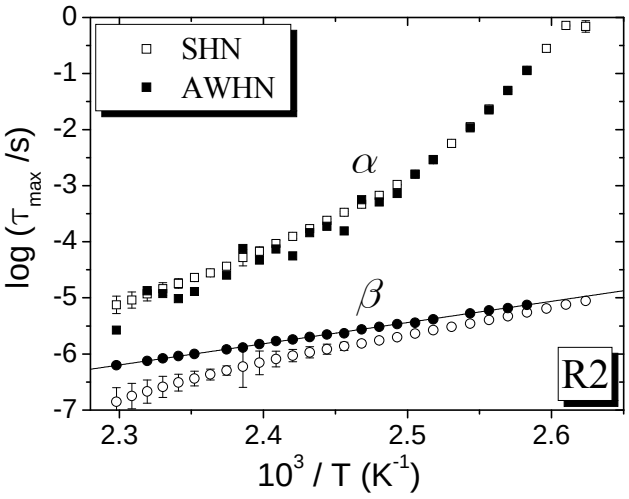

Figure 8.

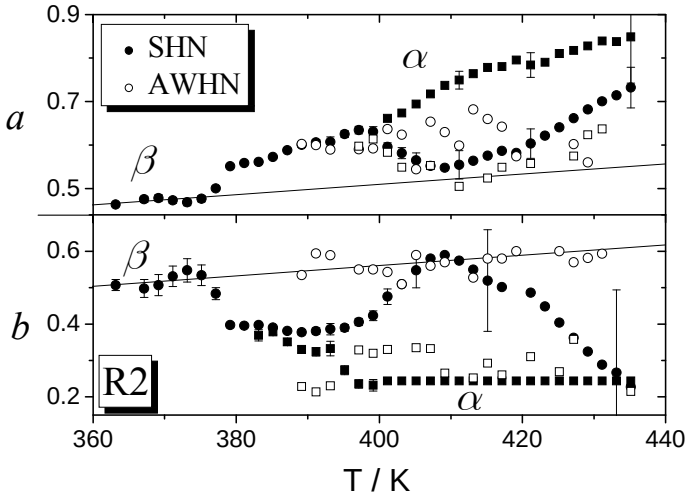

Figure 9.

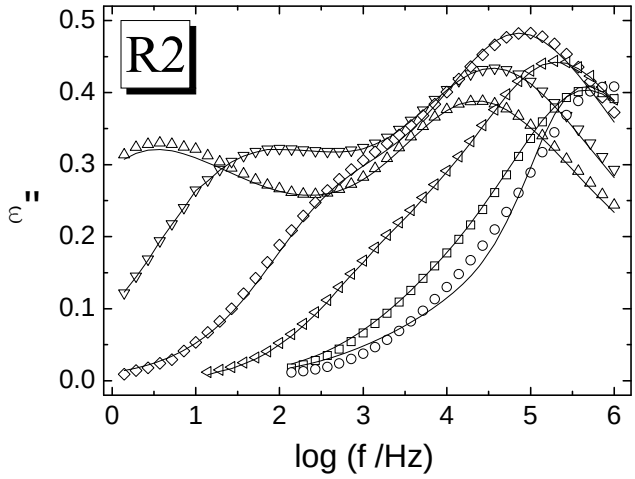

Figure 10.

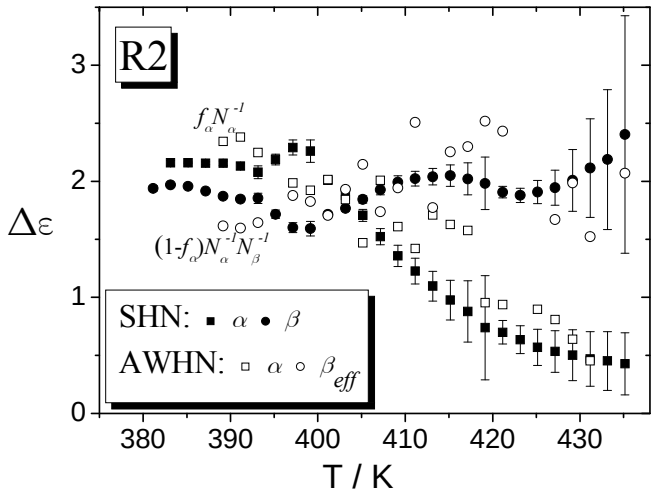

Figure 11.

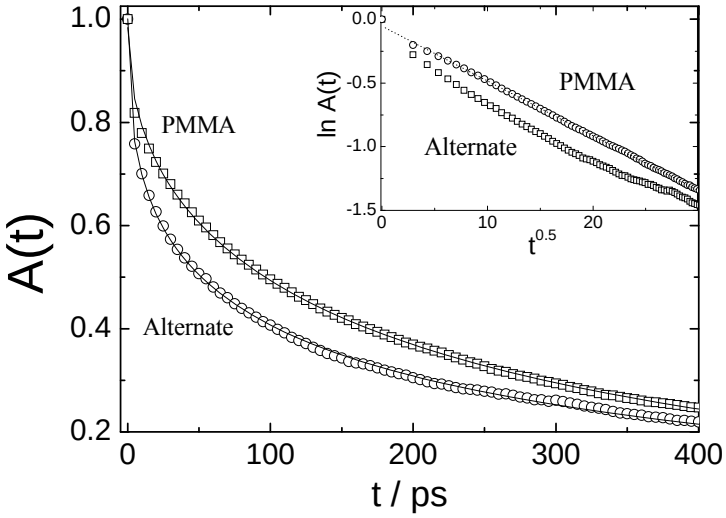

Figure 12.

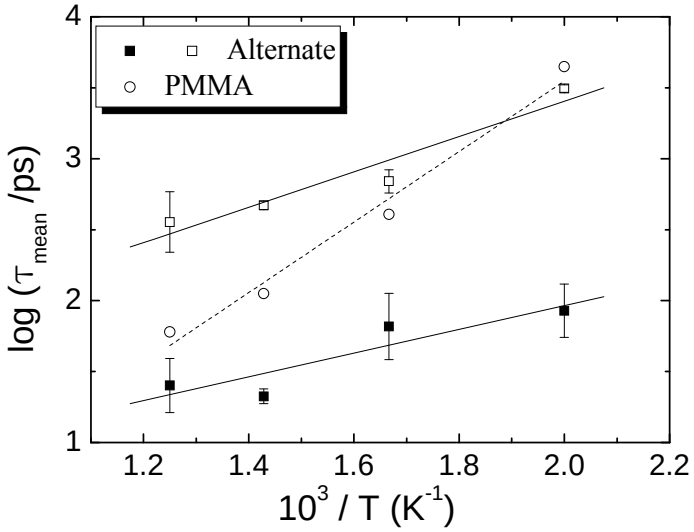

Figure 13.